STUDY ON AERODYNAMIC SOUND GENERATION BY VORTEX MOTIONS IN A CIRCULAR JET

Riho Hiramoto, Kuniaki Toyoda and Hayato Mori
Department of Mechanical Systems Engineering,
Hokkaido Institute of Technology
Maeda 7-15-4-1, Teine-ku, Sapporo 006-8585, Japan
hiramoto@hit.ac.jp, toyoda@hit.ac.jp

ABSTRACT

Simultaneous measurements of velocity and fluctuating static-pressure were carried out in an air jet issuing from a sharp-edged circular orifice, and the sound source terms of vortex sound theory and dilatation theory were discussed in relation to the vortex motions. The jet was excited in the interaction mode so that velocity and fluctuating static-pressure can be determined in space and time domains by using phase-average technique. The sound source terms of the theories were obtained from the phase-average velocity and fluctuating static-pressure via the differential process in space and time. The result suggests that intense sound sources are caused by the vortex merging and by the acceleration of vortices during vortex pairing. In addition, it is noted that the regions of intense sound source are different from those of intense fluctuating-velocity and -pressure.

INTRODUCTION

The aerodynamic sound is closely related to the vortex motions, as indicated by the 'vortex sound theory' (Powell, 1964, Howe, 1975). Many research works have been reported about the jet noise generation focusing on the relation between the aerodynamic sound generation and the vortex motions. There have been several candidates suggested on the generation mechanism of aerodynamic sound: rolling-up and merging of vortices (Laufer et al., 1973, Ffowcs and Kempton, 1978, Colonius et al., 1997, Li et al., 2000), break-down of a vortex ring via cut-and-connect process (Takaki and Hussain, 1985), interactions of vortices (Kambe, 1986) and stretching of vortex filament (Ishii et al., 1997). Thus, in order to control the jet noise, it is crucial to make clear the relations between the vortex motions and the sound sources.

The vortex sound theory is expressed on the assumption of very small Mach number:

$$\frac{1}{c_0^2}\frac{\partial^2 p'}{\partial t^2} - \nabla^2 p' = \rho_0 \,\mathrm{div}\,(\boldsymbol{\omega} \times \boldsymbol{u}) \qquad (1)$$

where c_0 is the sound speed, p' is the sound pressure in far-field, ρ_0 is the mean density of fluid, $\boldsymbol{\omega}$ is the vorticity vector and $\boldsymbol{u}$ is the velocity vector. The sound source term on the right-hand side suggests that the existence of vorticity is necessary for the aerodynamic sound generation. In particular, it is expected that the unsteady vortex motions mentioned above play an important role for the sound generation.

In the experimental works, the vortical structures are usually detected by measuring vorticity from velocity data. However the results have serious errors owing to the structure 'jitter' and to the differential process required in the vorticity measurement. Moreover it is very hard to detect the three-dimensional vortical structures in turbulent flows by the vorticity measurement.

The vortical structures are closely related to the instantaneous pressure as shown by the Poisson's equation for pressure:

$$-\frac{1}{\rho_0}\nabla^2 p = \frac{\varepsilon}{2\nu} - \frac{1}{2}\omega_i^2 \qquad (2)$$

where p is the instantaneous pressure, ε is the instantaneous dissipation, ν is the kinematic viscosity and ω_i is the instantaneous vorticity. This equation indicates that the vorticity contributes to $\nabla^2 p$ being positive (Bradshaw and Koh, 1981): the low-pressure region including a minimum pressure point is closely related to the vorticity-concentrated region. Indeed the results of direct numerical simulation (Kasagi et al., 1995) reveal that the low-pressure regions in the fluctuating pressure field correspond to the vortical structures. Thus the detailed pressure measurements in turbulent flows are expected to give us useful information on the vortical structures. Another advantage is that, since pressure is scalar, the pressure measurements are useful to detect three-dimensional vortical structures.

Although a significance of the pressure fluctuations in turbulent flows has been pointed out, there have been few works on the direct pressure measurements which are usually attended with serious errors due to the disturbance caused by a pressure probe inserted in flows. Toyoda et al. (1994) developed a probe to measure the fluctuating static pressure in turbulent flows, and confirmed that the direct pressure measurements with the probe are very effective to detect the three-

dimensional large-scale vortical structures in jets (Toyoda and Hiramoto, 1999).

The pressure fluctuations are also closely related to the sound source of turbulent flows. Ribner (1962) proposed a theory of aerodynamic sound, called 'dilatation theory', developing Lighthill's equation (Lighthill, 1952). The Ribner's equation is deduced on the assumption of Mach number $M \rightarrow 0$:

$$\frac{1}{c_0^2}\frac{\partial^2 p^{(1)}}{\partial t^2} - \nabla^2 p^{(1)} = -\frac{1}{c_0^2}\frac{\partial^2 p^{(0)}}{\partial t^2} \qquad (3)$$

where $p^{(0)}$ is the local pressure in flow and $p^{(1)}$ is the sound pressure. The sound source term in the right-hand side is the second time derivative of $p^{(0)}$.

As mentioned above, pressure is closely related to vortical structures and sound source in flows, and the pressure measurements are useful to detect both of them. In the present study, the vortex motions and the sound sources of the sound generation theories are detected by simultaneous measurements of velocity and pressure fluctuation in a circular jet, and the generation mechanism of jet sound is discussed in relation to vortex motions.

EXPERIMENTAL APPARATUS

The wind tunnel used in the experiments is shown in Fig.1. The air was issued from a circular orifice. The diameter of the circular orifice De is 50mm, the velocity Ue at the jet exit center is 4 m/s, and the Reynolds number Re (=Ue·De/ν) is 1.3×10^4.

The jet was excited by a loudspeaker at the side of settling chamber of the wind tunnel. The circular jet was excited at an eighth of the natural frequency of the shear layer generating from the orifice edge without excitation. The Strouhal number is 0.82. The excitation intensity u'/Ue (u': the rms value of fluctuating velocity) at the jet exit center was 3%. Under the excitation, stable vortex pairing was produced at the same spatial station at regular intervals.

The pressure probe to measure fluctuating static-pressure is shown in Fig. 2. The static-pressure tube with four small holes connected at the end to the condenser microphone. The structure and the dimension of the probe were determined so as to minimize errors in the measurements of fluctuating static-pressure. In order to damp the organ pipe resonance in the tube, a thin nylon gauze was inserted in front of the diaphragm of microphone, and the probe had a nearly flat frequency resonance to 2.0 kHz. The cross-flow error of the static pressure tube was calibrated in the uniform flow by changing the flow attack angle to the tube. The pressure drop of the present tube is less than that of a standard one over the wide range of attack angle (Toyoda and Hiramoto, 1999). The dynamic response of the probe is discussed by Toyoda et al. (1994)

The combined sensor of X-type hot-wire and pressure probes in Fig. 3 was used to measure velocity and fluctuating static-pressure simultaneously. The distance between sensing positions of two probes was 2mm, which is a minimum distance to neglect the interaction of hot-wire and pressure probes.

The coordinate system and the arrangement of the probes for the phase-average measurement is shown in Fig. 4. The reference velocity was measured by a single normal hot-wire probe fixed near the jet center at x/D ≒ 1.0, and velocity and

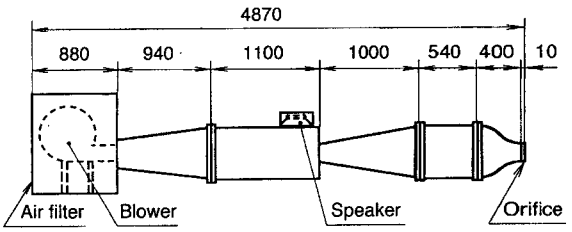

Fig.1 Wind tunnel

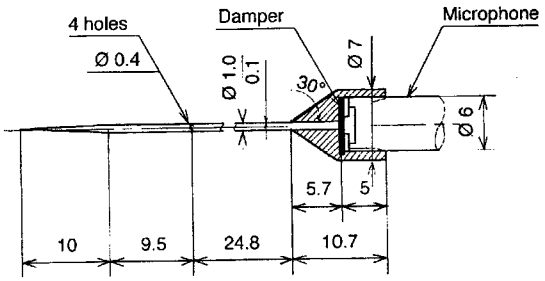

Fig.2 Pressure probe

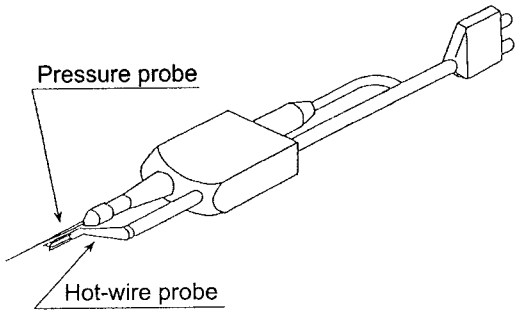

Fig.3 Combined sensor of x-type hot-wire and pressure probes

pressure fluctuations were measured by the combined sensor moving over the flow field. The traversing of the sensor, the data acquisition and the data processing were automatically controlled by personal computers.

DATA PROCESSING

The phase-averaging of velocity and fluctuating static pressure was carried out at 36 phase angles of the reference signal from $\theta=0$ to $\theta=2\pi$ with an increment of $\pi/18$ (see Fig. 5). The sampling number for phase-averaging is about 200 at each phase. Non-dimensionalized phase-average velocity $<\boldsymbol{u}>$, vorticity $<\omega_z>$, fluctuating static-pressure $<p^{(0)}>$, sound source term of the 'vortex sound theory' $<\mathrm{div}(\boldsymbol{\omega}\times\boldsymbol{u})>$ and sound source term of the 'dilatation theory' $<-\partial^2 p^{(0)}/\partial t^2>$ are defined by

$$<\boldsymbol{u}> \equiv [\boldsymbol{u}]_p / \mathrm{Ue} \qquad (4)$$

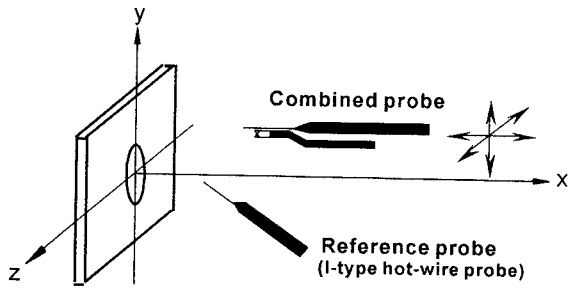

Fig.4 Coordinate system and arrangement of probes of phase-average measurement

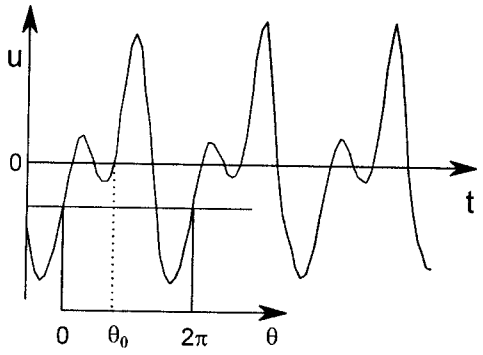

Fig.5 Reference signal

$$<\omega_z> \equiv \left(\frac{\partial [v]_p}{\partial x} - \frac{\partial [u]_p}{\partial y} \right) / (Ue/De) \quad (5)$$

$$<p^{(0)}> \equiv 2[p^{(0)}]_p / \rho Ue^2 \quad (6)$$

$$< \mathrm{div}(\boldsymbol{\omega} \times \boldsymbol{u}) > \equiv \mathrm{div}(<\boldsymbol{\omega}> \times <\boldsymbol{u}>) De \quad (7)$$

$$<-\partial^2 p^{(0)}/\partial t^2> \equiv 2[-\partial^2 p^{(0)}/\partial t^2]_p / (\rho_0 Ue^4/De^2) \quad (8)$$

where $[\ ]_p$ designates a phase-average value.

RESULTS

Vorticity and Fluctuating Static-Pressure

The contours of phase-average vorticity and fluctuating static-pressure in the xy plane are shown in Fig. 6. The contours are presented at six phases with an increment of $\pi/3$; the phase increases from the top to the bottom. The frames (1)-(6) indicates one cycle of the periodic vortex motion. The negative-pressure regions of $<p^{(0)}>$ contours (Fig.6 (b)) correspond to the vorticity concentrated regions (Fig. 6 (a)). The contours show how the leading (L_1, L_2 and L) and trailing (T) vortices interact each other. The leading vortices (L_1 and L_2) come out from the left-hand side (frame (1)) and merge at x/d $\approx$ 1.2 (L in frame (3)). The trailing vortex (T) rushes inside the leading vortex (L) as shown in frames (4)-(6). The leading and the trailing vortices merge at x/d $\approx$ 2.2 farther downstream.

Comparing the contours in Fig. 6 (a) and (b) from the viewpoint of detecting the vortical structure, the low pressure field seems to show vortices distinctly rather than the vorticity field, particularly downstream as shown in frames (6), which correspond to the phase after the trailing vortex passes inside the leading vortex. This difference maybe comes from the differential process required in the vorticity calculation and additionally from the dissipation term in Eq. (2).

Sound Sources

Figure 7 (a) and (b) show the contours of phase-average sound source terms of the vortex sound theory, $< \mathrm{div}(\boldsymbol{\omega} \times \boldsymbol{u}) >$ and of the dilatation theory, $<-\partial^2 p^{(0)}/\partial t^2>$. The phases of the frames (1)-(6) in Fig. 7 correspond to those in Fig. 6. By comparing Figs. 7 and 6, we can understand the relation between the sound sources and the vortex motions: the intense regions of sound source locate just around the vorticity concentrated regions. In particular, positive and negative regions in Fig. 7 (a) locate respectively on inner and outer sides of the vorticity concentrated regions. In addition, while the trailing vortex rushes inside the leading vortex in frames (1), (4) and (5), the intensity of the sound sources related to the trailing vortices become higher than those related to the leading vortices.

In Fig. 7 (b), the negative regions correspond to the vorticity concentrated regions in Fig.6 (a) and the low pressure regions in Fig.6 (b), and the positive regions are located on both sides of the negative regions in the direction of vortex convection. Through out the vortex pairing event, the intensity of sound source related to the trailing vortex is higher than that related to the leading vortex. This feature is consistent with the case of vortex sound theory in Fig.7 (a).

From the contours in Fig. 7 (b), it is reasonably understood that the distribution of the sound source term $<-\partial^2 p^{(0)}/\partial t^2>$ is closely related to the vortex convection: when the trailing vortex passes inside the leading vortex, it is accelerated by the induced velocity of the leading vortex, and the sound source is intense. On the contrary, the leading vortex is decelerated by the induced velocity of the trailing vortex, and the sound source is weak relatively.

Intensity of Fluctuations

The instance relations between vortex motion and sound source are revealed as shown in Fig. 6 and 7. In order to discuss locations of the sound generation in the circular jet, the intensities of both sound sources, $< \mathrm{div}(\boldsymbol{\omega} \times \boldsymbol{u}) >_{rms}$ and $<-\partial^2 p^{(0)}/\partial t^2>_{rms}$, are calculated with the results in Fig.7. The intensity was defined by rms value of the periodic motion as expressed by $<f>_{rms}$, which is calculated with the phase-average value. The intensities of the sound sources are shown in Figs. 8 in comparison with those of vorticity and pressure fluctuation.

The high intensity regions of $<\omega_z>_{rms}$ in Fig. 8 (a) correspond to the trajectories of the leading and the trailing vortices. On the other hand, the intense region of $<p^{(0)}>_{rms}$ in Fig. 8 (b) corresponds to the trajectory of the leading vortex. The intense region of $< \mathrm{div}(\boldsymbol{\omega} \times \boldsymbol{u}) >_{rms}$ in Fig. 8 (c) is similar to that of $<\omega_z>_{rms}$ particularly upstream (at x/De < 1.25). In Fig. 8 (d), the intense region of $<-\partial^2 p^{(0)}/\partial t^2>_{rms}$, related to the trailing vortex, is distinct. Due to the characteristics of the sound source term $<-\partial^2 p^{(0)}/\partial t^2>$, the higher velocity of vortex convection leads to the intense sound source as described in previous section. Figure 8 reveals that the intense sound sources are generated by the vortex merging of L_1 and L_2

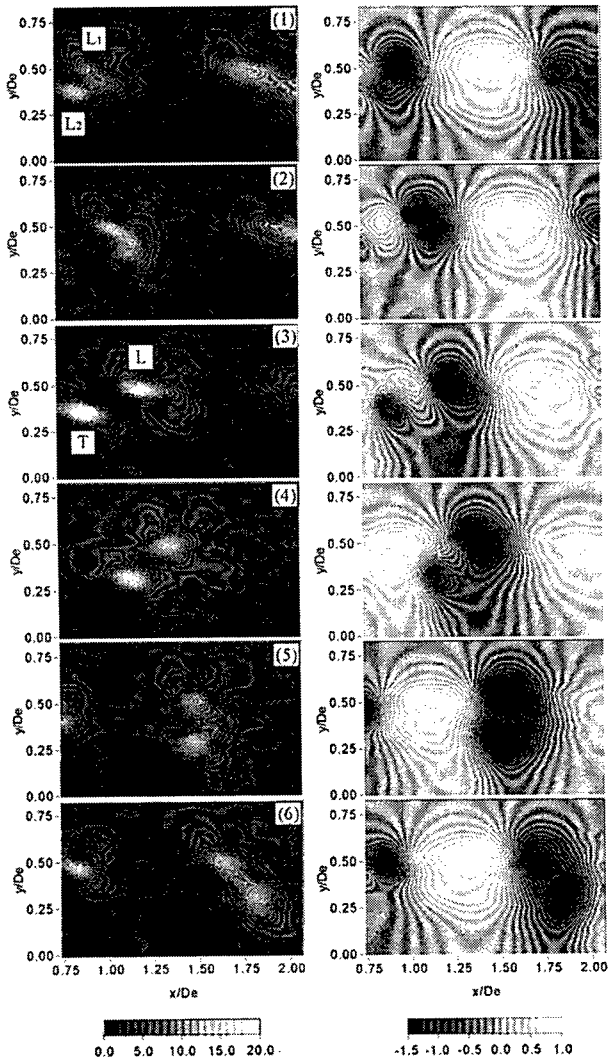

(a) $< \omega_z >$ (b) $<p^{(0)}>$

Fig.6 Contours of phase-average vorticity and fluctuating static-pressure

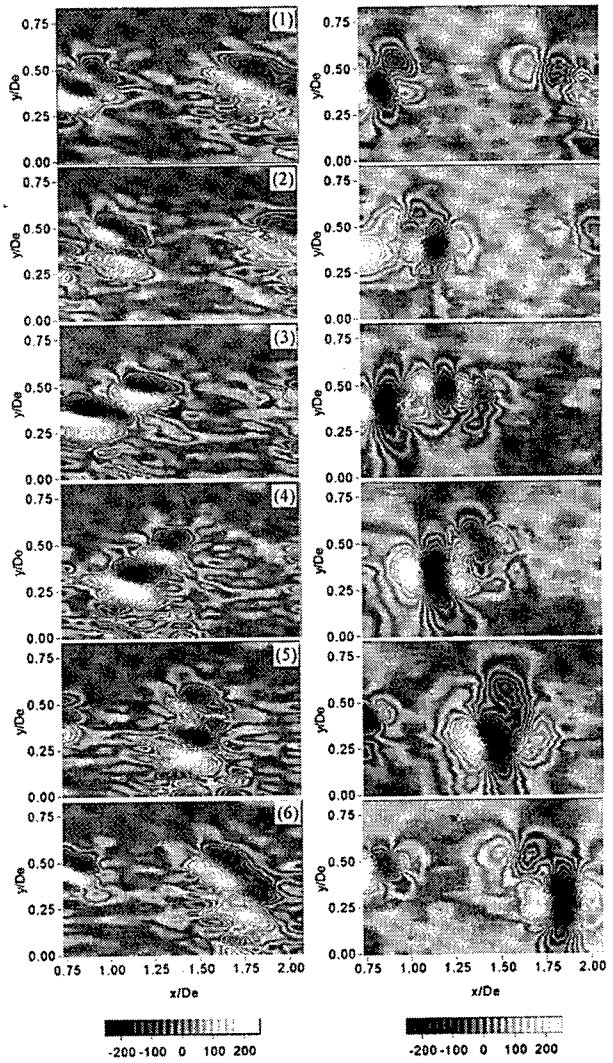

(a) $< \mathrm{div}\,(\boldsymbol{\omega} \times \boldsymbol{u}) >$ (b) $<-\partial^2 p^{(0)}/\partial t^2>$

Fig.7 Contours of phase-average sound source

from the frame (2) to the frame (3) in Fig. 6 and by the vortex pairing downstream.

In practical measurements, it is usual to measure velocity fluctuations by hot-wire anemometry to discuss the characteristics of the sound source in stead of detecting sound source term directly. As we recognized the difference between the distributions of $<p^{(0)}>_{rms}$ and $<-\partial^2 p^{(0)}/\partial t^2>_{rms}$ unexpectedly, it is important to check the relation between the velocity fluctuations and the sound source. The intensity of fluctuating velocity of x- and y-components are shown in Fig. 9 (a) and (b) respectively. Two intense regions in Fig. 9 (a) are related to the leading and the trailing vortices. The regions deviate slightly from those in Fig. 8 (a) and (c): the former is inside of the vortex trajectories. The reason is that the induced velocity by the convected vortex increases the inside velocity and decreases the outside velocity.

On the other hand, in Fig. 9 (b), the intense region related to the leading vortex is distinct rather than that related to the trailing vortex. The locations of maximum intensity are at x/De $\approx$ 1.0 and 1.5, where the trailing vortex passes just inside of the leading vortex during the pairing event.

DISCUSSIONS

Distributions of the Sound Source

Positive and negative regions of the sound source of the vortex sound theory locate respectively on inner and outer sides of the vorticity concentrated regions as shown in Fig. 7(a). The generating mechanism of the sound source is discussed here with experimental data.

The sound source term of vortex sound theory in xy-plane is as follows.

$$\mathrm{div}(\boldsymbol{\omega}\times\boldsymbol{u}) = -\frac{\partial \omega_z v}{\partial x} + \frac{\partial \omega_z u}{\partial y} \qquad (9)$$

The distributions of the sound source term $\mathrm{div}(\boldsymbol{\omega}\times\boldsymbol{u})$ in the actual results mostly depend on the second term on right-hand side of Eq. (9), not shown here. Then we focus on the components effecting on the second term.

Figure 10 shows instantaneous velocity fields at x/De=1.2 of the frame(3) in Figs. 6 and 7. Figures 10(a) and (b) present

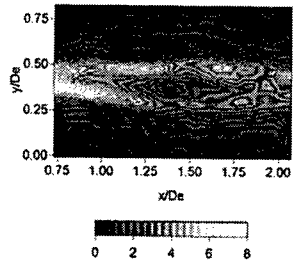

$<\omega_z>_{rms}$

(a) Intensity of vorticity

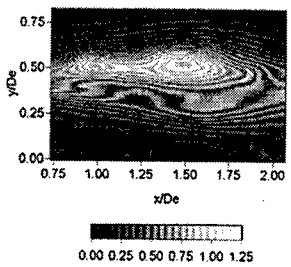

$<p^{(0)}>_{rms}$

(b) Intensity of fluctuating static-pressure

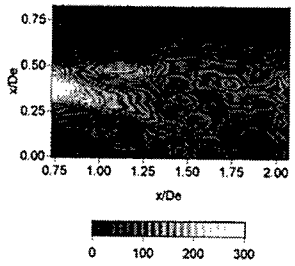

$< \mathrm{div}(\boldsymbol{\omega} \times \boldsymbol{u}) >_{rms}$

(c) Intensity of sound source of Vortex sound theory

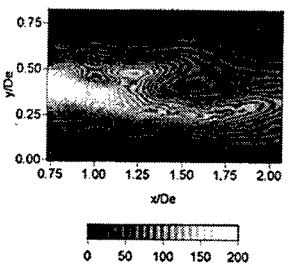

$<-\partial^2 p^{(0)}/\partial t^2>_{rms}$

(d) Intensity of sound source of Dilatation theory

Fig.8 Intensity of vorticity, fluctuating static-pressure and sound sources of vortex sound theory and dilatation theory

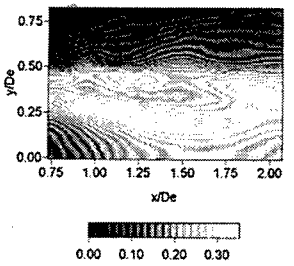

u'/Ue

(a) x-component fluctuating velocity

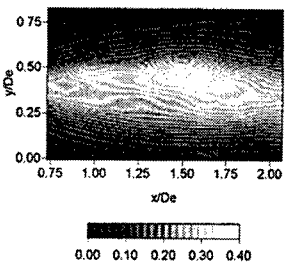

v'/Ue

(b) y-component fluctuating velocity

Fig.9 Turbulence intensity

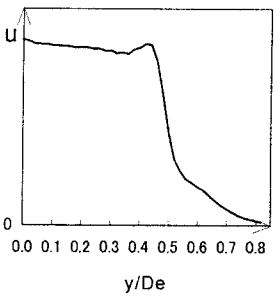

(a) Velocity

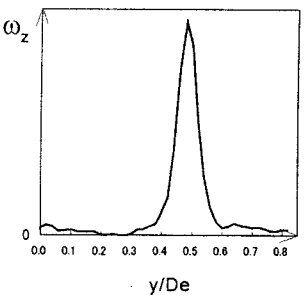

(b) Vorticity

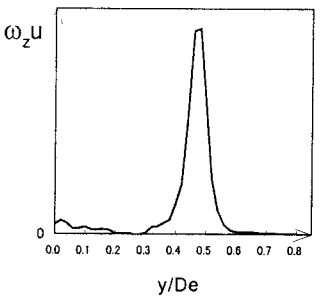

(c) $\omega_z u$

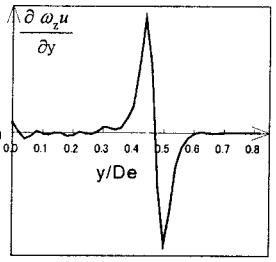

(d) $\frac{\partial \omega_z u}{\partial y}$

Fig.10 Velocity fields (x/De=1.2, corresponding to the frame (3) in Fig.6(a))

the instantaneous velocity and vorticity distributions. There is a hump in Fig.10(a) caused by the induced velocity of the vortex ring. Figure 10(c) and (d) show $\omega_z u$ and $\partial\, \omega_z u / \partial y$ respectively. Since the values of ω_z and $\omega_z u$ have maxima at the same position, the sign of $\partial\, \omega_z u / \partial y$ changes at the maximum point of ω_z: $\partial\, \omega_z u / \partial y$ is positive on the inside of the vortex ring and negative on the outside.

The sound source distribution around vortex in the jet is different from that of the numerical simulation (Li et al., 2000) on the sound generation in a plane mixing layer: the sign of the sound source term is negative in the inner region of vortex and positive in the outer region.

In the mixing layers, the humps of velocity profile occur on both sides of vortex in the y-direction (Li et al., 2000). The humps cause negative gradient of $\omega_z u$ in the inner region of vortex and positive gradient in the outer region, leading to the sign of the sound source term mentioned.

The above discussion shows that the difference between the sound source distributions of the present circular jet and the mixing layers (Li et al., 2000) is due to the difference of velocity profiles. The velocity profiles are affected by induced velocity of vortices: in the circular jet a vortex ring generates a hump inside, and in the mixing layer a vortex generates humps on both sides of the vortex.

In the sound source distribution of the dilatation theory (Fig.7(b)), the negative regions correspond to the vorticity concentrated regions and the positive regions are located on both sides of the negative regions in the direction of vortex convection. The reason of the distribution can be explained with a simple model of pressure variation related to the vortex convection. An isolated vortex has low pressure region inside, and vortex convection produces pressure variation in time at a fixed station as shown in Fig.11(a). The second time-derivative of pressure $p^{(0)}$, the sound source term of the dilatation theory, is shown in Fig.11(b): the sign changes positive, negative and again positive in time.

Variation of Sound Source Intensity with Phase

As shown in Figs.6 and 8, the sound source generation is

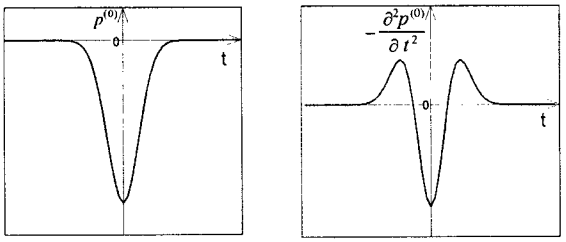

(a) Pressure (b) Sound source term

Fig.11 Models of variation of pressure fields

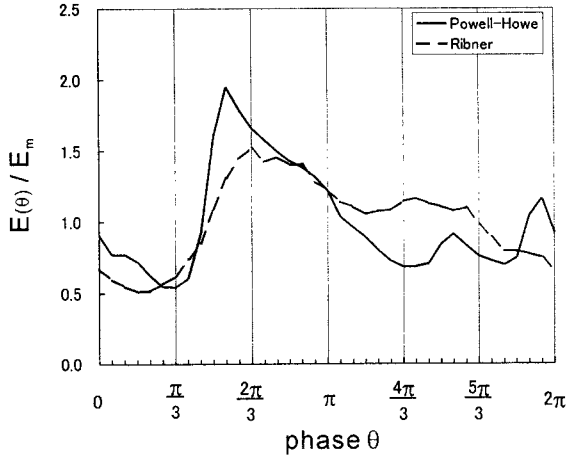

Fig.12 Time variation of the integrated sound source terms

closely related to the vortex motion at each phase. In order to discuss the variation of the sound source intensity with phase, we calculated the integrated value of the sound source intensity at each phase by the following equation.

$$E(\theta) = \int\int_A T_\theta(x, y)^2 \, dxdy \qquad (10)$$

where θ is the phase, $T_\theta(x, y)$ is the sound source term, $< \mathrm{div}(\boldsymbol{\omega} \times \boldsymbol{u}) >$ or $<-\partial^2 p^{(0)}/\partial t^2>$, at a phase, and A is the measured region. $\theta = 0$ corresponds to the frame(1) in Fig.7, and $E(\theta)$ is calculated for 36 phases. $T_\theta(x, y)^2$ is integrated over the measured region shown in Fig.7.

The variation of non-dimensional $E(\theta)$ is shown in Fig.12, where is E_m is the mean value of $E(\theta)$. The figure shows that the variations of $E(\theta) / E_m$ calculated by two sound source theories are similar. The result suggests that the sound source of Ribner's equation corresponds to that of the vortex sound theory qualitatively.

CONCLUSIONS

The simultaneous measurements of velocity and fluctuating static-pressure were carried out in a circular jet, and the sound source terms of the vortex sound theory and the dilatation theory were discussed in relation to the vortex motions.

The results suggest that the generation of the sound sources is closely related to vortex motions. In particular, the intense sound sources are generated by the vortex merging and by the accelerated vortex motion during vortex pairing.

The characteristics of the sound source distributions are discussed in relation to vortex motion: the induced velocity of vortices and the vortex convection influence the signs of the sound source terms.

REFERENCES

Bradshaw, P. and Koh, Y. M., 1981, "A note on Poisson's equation for pressure in a turbulent flow", *Phys. Fluids*, Vol. 24, pp. 777.

Colonius, T., Lele, S. K. and Moin, P., 1997, "Sound generation in a mixing layer", *J. Fluid Mech.*, Vol. 330, pp. 375-409.

Ffowcs Williams, J. E. and Kempton, A. J., 1978, "The noise from the large-scale structure of a jet", *J. Fluid Mech.*, vol. 84, pp. 673-694.

Howe, M. S., 1975, "Contribution to the theory of aerodynamic sound, with application to excess jet noise and the theory of the flute", *J. Fluid Mech.*, Vol. 71, pp. 625-673.

Ishii, K., Adachi, S. and Maru, H., 1997, "Numerical estimation of vortex sound from Oblique between vortex rings (II)", *29th Symposium on Turbulence*, Japan, pp. 271-272.

Kambe, T., 1986, "Acoustic emissions by vortex motions", *J. Fluid Mech.*, Vol. 173, pp. 643-666.

Kasagi, N., Sumitani, Y., Suzuki, Y. and Iida, O., 1995, "Kinematics of the quasi-coherent vortical structure in near-wall turbulence", *J. Heat Fluid Flow*, Vol. 16, pp. 2-10.

Laufer, J. et al., 1973, "On the generation of jet noise", *AGARD CP-131*, Pap. 21.

Lighthill, M. J., 1952, "On sound generated aerodynamically, I. General theory", *Proc. Roy. Soc London*, A211, pp. 564-587.

Li, Y., Tanahashi, M. and Miyauchi, T., 2000, "Sound generation in compressible mixing layers", *Trans. of the Japan Soci. Mechanical Engineers* (in Japanese), Vol. 66, 1527-1534.

Powell, A., 1964, "Theory of vortex sound", *J. Acoust. Soc. Am.*, 33-1, pp. 177-195.

Ribner, M. S., 1962, "Aerodynamic sound from fluid dilatation", *Univ. Tronto. Inst. of Aerodynamics Report*, No. 86, 1962.

Takaki, R. and Hussain, A. K. M. F., 1985, "Recombination of vortex filaments and its role in aerodynamic noise", *5th Symp. on Turbulent Shear Flows*, Cornell Univ., USA, 3.19-3.25, August 7-9, 1985.

Toyoda, K., Okamoto, T. and Shirahama, Y., 1994, "Eduction of Vortical Structures by Pressure Measurements in Noncircular Jets", *Appl. Scientific Res.*, Vol. 53, pp. 237-248.

Toyoda,K. and Hiramoto,R., 1999, "Vortical structure and diffusion mechanism of a rectangular jet", 3rd ASME/JSME Joint Fluids Eng. Conf., FEDSM99-6946.